Failure warning of hydrous sandstone based on electroencephalogram technique

Kai Tao, and *Wei Zheng* *

College of Optoelectronic Engineering, Chongqing University, Chongqing, 400044, China

Abstract. Sandstone is a type of rock mass that widely exists in nature. Moisture is an important factor that leads to sandstone structural failure. The major failure assessment methods of hydrous sandstone at present cannot satisfy real-time and portability requirements, especially lacks of warning function. In this study, acoustic emission (AE) and computed tomography (CT) techniques are combined for real-time failure assessment of hydrous sandstone. Eight visual colors for warning are screened according to different failure states, and an electroencephalogram (EEG) experiment is conducted to demonstrate their diverse excitations of the human brain's concentration.

1 Introduction

Acoustic emission (AE) of rocks is a phenomenon in which cracks inside a rock develop high energy under local stress and release energy to achieve a stable state by generating transient elastic waves [1]. Sandstone, which is mainly composed of quartz and feldspar, is a common rock type in geotechnical engineering. Moisture can change the physical properties of sandstone particles and soften loading resistance. Stability is also affected, and this scenario leads to different levels of failure [2-3].

In this study, Failure assessment was completed in real time when AE signals were collected. A visual warning mechanism of assessment results was established based on EEG.

2 Mapping rule of AE and moisture through the SVM algorithm

Training samples with five types of moisture contents were obtained through a weighing method. The moisture contents were 0%, 25%, 50%, 75%, and 100%. The AE signals of all samples were collected, and the energy and duration parameters were extracted afterward. The mapping rule of AE and moisture was obtained using an SVM classifier. The original energy and duration parameters are shown in Figure 1(a) and (b), where the horizontal axis is a random sample number and the vertical axis is the value of a characteristic parameter. Of the 100 samples for each moisture content, 70 were used as training groups, and the rest (30 samples) were utilized as test groups. The C-SVC structure network and linear kernel function were used to verify the SVM classifier's identification of the effect of different moisture contents. The identification result is shown in Figure 1(c).

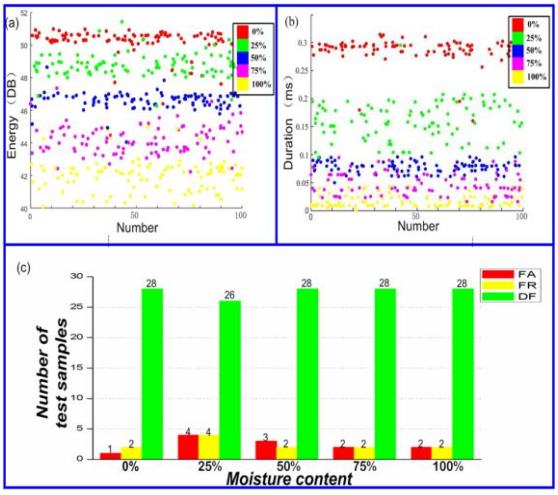

Fig. 1. (a) and (b) Original data of energy and duration parameters. (c)Moisture content identification result of SVM

According to the numbers of false acceptance (FA; classified into the same level but the actual moisture is different), false rejection (FR; not classified into the same level but the actual moisture is the same), and discriminant formula (DF; classified into the same level and the actual moisture is the same), which are displayed in the diagram, 138 were classified correctly, and the overall identification accuracy of SVM was 92%. Aside from the efficacy of the network structure, the significant difference in AE parameters with diverse moisture was also an important factor for the high identification accuracy. This result indicates the feasibility and rationality of this method.

3 Mapping rule of moisture and failure level through CT technique

* Wei Zheng: zw3475@163.com

3.1 Comprehensive index failure assessment of sandstone

(1) Morphologic quantification of cracks

The morphologic information (such as area, length, and width) of cracks can be quantificated on the CT image after the connected domain-quantifying filtering [4-5]. The number of elements, which are incorporated into the slit region, can be calculated as the area A_c of this region. Skeleton extraction can be employed to obtain the eigenvalue of the crack image and the number of pixels L_c in the skeleton diagrams is the crack length. The average width of a crack can be calculated using Eq. 1.

$$W_c = A_c / L_c \tag{1}$$

The above crack's morphological parameters are aimed toward a single crack. If the rock surface has many cracks or a bifurcation phenomenon exists, then the cracks should be numbered, the area, length, and width of a single crack should be calculated, and all crack parameters should be summed up. We assume that the number of sandstone cracks is n, and the area, length, and width of a single crack are $A_{c_i}^{'}$, $L_{c_i}^{'}$, and $W_{c_i}^{'}$, respectively, where $i \in (1,n)$. For the sample crack, $A_c = \sum_{i=1}^{n} A_{c_i}^{'}$, $L_c = \sum_{i=1}^{n} L_{c_i}^{'}$, $W_c = \frac{1}{n}\sum_{i=1}^{n} W_{c_i}^{'}$.

(2) Comprehensive failure index

To present the failure information of rock mass in many aspects, the following three failure morphological indexes are defined based on reference [6].

$$\alpha = A_c / A_R \ , \quad \beta = L_c^{\,2} / A_c \ , \quad \gamma = W_c^{\,2} / A_c \tag{2}$$

where A_R is the area of the CT image; A_c, L_c, and W_c are the area, length, and width of the crack, respectively. Parameter α reflects the overall failure degree of the rock mass, β reflects the longitudinal expansion of the crack, and γ reflects the transverse expansion of the crack.

Given the different physical properties of materials, the diversity of crack expansion is obvious. To describe the rock failure scientifically, a comprehensive index is provided as follows:

$$\phi = \omega_1 * \varepsilon_1 * \alpha + \omega_2 * \varepsilon_2 * \beta + \omega_3 * \varepsilon_3 * \gamma \tag{3}$$

where ω_1, ω_2, and ω_3 are the weight of the three morphological failure indexes, and $\omega_1 + \omega_2 + \omega_3 = 1$. The specific value reflects the diversity of crack expansion tendency and varies according to different materials. Significant diversity exists in the trend of crack expansion due to the difference in the rock particles' physical properties. For example, the consistency of sandstone particles is obvious, and the expansion degree of cracks is uniform in each direction. Thus, the difference in crack length and width is small among the three weights. However, the longitudinal trend of crack is highly obvious due to the lamellar joints. Hence, the crack is long, and parameter is large. The magnitudes of the three indexes are different, but all of the indexes require the same magnitude. Thus, magnitude adjustment coefficients ε_1, ε_2, and ε_3 were set to adjust the magnitudes into the same interval. The specific values were determined by the rock crack propagation characteristics.

3.2 Failure assessment rule table

The failure level of rocks is defined from one to four grades, and the failure intensifies with the increase in value. Moisture reduces the compression capability of sandstone and increases the expansion trend of failure cracks [7]. Therefore, the comprehensive failure index of the saturated and extremely failured sample was used as a basis. This value is divided into four equal parts, which are regarded as a judging rule for failure assessment. The weight of the three morphological failure indexes was 0.33, and magnitude adjustment coefficients ε_1, ε_2, and ε_3 were set to 100, 0.1, and 100, respectively. The calculated value of ϕ is 9.91, and the failure assessment rule table is shown in table 1.

Table 1. Failure assessment rule table.

Failure level	comprehensive failure index interval
First level	[0,2.48)
Second level	[2.48,4.96)
Third level	[4.96,7.44)
Fourth level	[7.44,9.91]

3.3 Mapping rule of moisture and failure level

By calculating the morphological parameters and comprehensive index of the five crack images, the failure level of each moisture was classified according to the rule table of failure assessment, as shown in table 2.

Table 2. Failure classification of different moisture samples.

Moisture content	α	β	γ	ϕ	Failure level
0%	0	0	0	0	First level
25%	0.014	27.57	0.036	2.56	Second level
50%	0.034	67.73	0.015	3.85	Second level
75%	0.051	105.21	0.0095	5.47	Third level
100%	0.047	116.41	0.086	8.23	Fourth level

4 Real-time failure assessment function

The external environment in actual geotechnical engineering is complicated. The moisture and loading state of sandstone may change simultaneously. The synergistic effect of moisture and accumulative loading should be considered to obtain the exact damage state. A real-time damage assessment function of hydrous sandstone was proposed by considering two pieces of information: the assessment level, which varies with the

time of single AE, and the superposition effect of many AE events. The function at time t during the sandstone failure expression is as follows:

$$Q(t) = \sum_{i=1}^{n} Q_i = \sum_{i=1}^{n} \chi_i * d \qquad (4)$$

where n is the number of AE events up to time t and Q_i is the failure increment caused by AE event i. Parameter d is the unit of failure increment, which can be simplified to 1 in the actual application of failure assessment. $\chi_i \in \{1,2,3,4\}$, which is the same value as the failure level decided by AE event i. According to the mapping rules between moisture content and failure state, the expression of Q_i is as follows:

$$Q_i = \begin{cases} d & C_i = 0\% \\ 2d & C_i = 25\% \,||\, C_i = 50\% \\ 3d & C_i = 75\% \\ 4d & C_i = 100\% \end{cases} \qquad (5)$$

where C_i is the moisture content that corresponds to AE event i.

5 Real-time visual warning based on EEG technique

The Beta wave (13–30 Hz) in the human forehead is the main reflection of the human mental state. This rhythm becomes highly obvious when humans are excited or focused; thus, the Beta wave is the major reference for human concentration assessment [8]. The stimuli provided by different colors can directly affect the Beta wave in EEG and bring diverse emotional expressions to the human brain, such as tension and relaxation [9-10]. To acquire the most scientific visual warning according to the failure level, red, orange, royal blue, rose red, green, yellow, violet, and blue were used as alternative colors to assess the Beta wave in EEG. The order of the colors was determined according to the Beta wave value under the stimulation of the different colors. Assuming that the color order of damage level from low to high is $Col_1, Col_2, ..., Col_8$, thresholds $\theta_1, \theta_2, ..., \theta_7$ are the color switching basis. Five volunteers with normal intelligence and no color blindness were recruited. The EEG signal under the stimulation of the eight colors was collected, and the Beta wave was extracted to obtain different excitations of the concentration of the human brain. To avoid sample errors caused by the emotional state of volunteers, three experiments were conducted on each volunteer, and the most stable data were selected. The acquisition device was from NeuroSky Company, and data transmission was completed via a PC with Bluetooth capability. The typical original EEG waveforms under different color stimulations are shown in Figure 2(a).

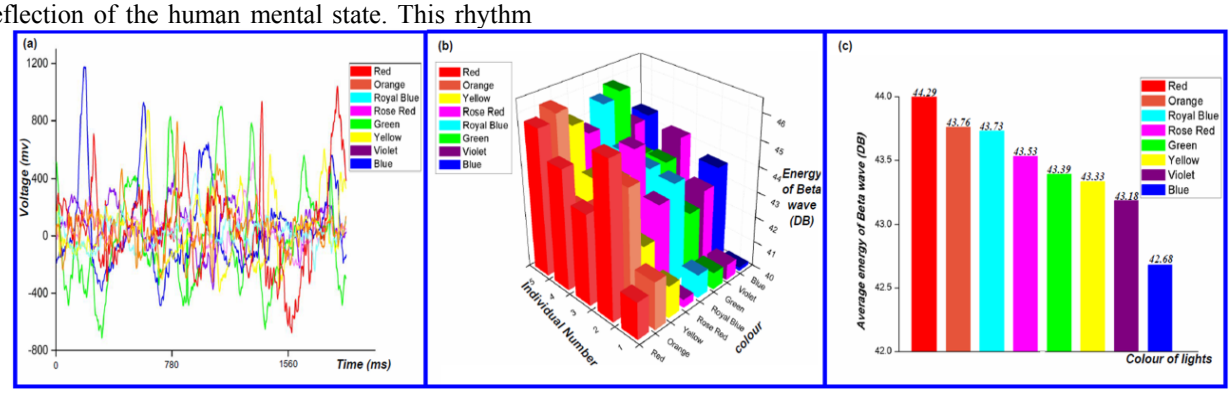

Fig. 2. (a) Typical original EEG waveforms under different color stimulations. (b) Beta wave energy in the EEG of five volunteers. (c) Average Beta wave energy of five volunteers

The original waveform shows that the morphological difference of EEG under diverse color stimulations is obvious. Hence, the concentration information of the human brain is difficult to observe directly. The Beta wave energy in the EEG of the five volunteers was extracted and is shown in Figure 2(b). The excitation regulation of the different colors on concentration was not identical due to the individual differences. However, warm colors, such as red and orange, were more likely to excite the Beta wave than cold colors, such as violet and blue. The average Beta wave energy under different color stimulations is shown in Figure 2(c). Red exerted the strongest excitation effect on the Beta wave in the EEG, which can lead to the maximum degree of concentration. Blue had the weakest effect. Hence, the visual warning order is blue, violet, yellow, green, rose red, royal blue, orange, and red according to the Beta wave excitation intensity.

6 Application experiment

To verify the feasibility of this real-time damage assessment method, an application test was conducted. First, slow-change uniaxial loading was applied to a dry sandstone sample. Its AE signal was collected, and the real-time damage state was assessed. Second, the moisture content was controlled up to 25%, and slow-change uniaxial loading was exerted on the sample without withdrawing the previous loading. The AE signal was collected, and the real-time damage state was assessed again. This step was repeated until the damage state of the 100% moisture sample was achieved. The visual warning color changed in real time during this process. The AE signals within 0-5 milliseconds were shown in Figure 3(a). The energy and duration parameters of the AE signal were extracted, and the

SVM classifier was used to realize AE–moisture mapping. The damage state in each of the different periods was calculated according to the moisture–damage level mapping rule and the real-time damage assessment function. The color switching failure thresholds were 10, 20, 30, 40, 50, 60, and 70. The failure state and visual warning color are shown in Figure 3(b).

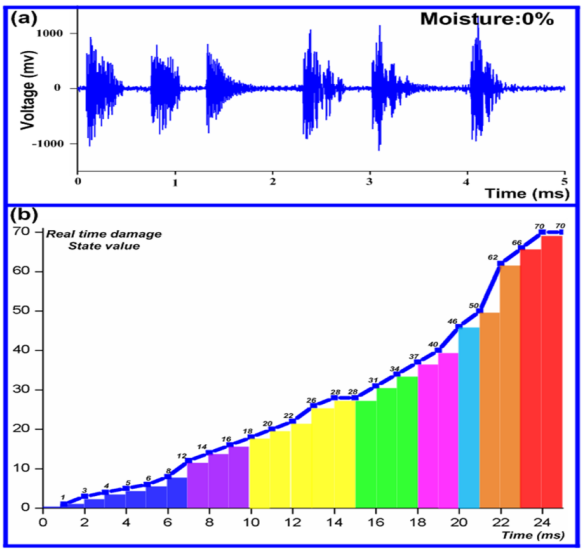

Fig. 3. (a) Original AE signals. (b) Real-time failure state and visual warning color

As shown in the figure, the damage state under the dual effect of moisture and loading can be obtained by the real-time damage assessment function, and the colors can be adjusted in real time. In actual geotechnical engineering, the change in moisture and loading can be very slow. Thus, the monitoring period is longer than that in this application test.

7 Conclusion

Hydrous sandstone failure plays an important role in geotechnical engineering safety. Currently, quantitative assessment of hydrous sandstone demonstrates poor real-time performance and insufficient portability, especially lacks of warning function. In this study, a failure assessment function of hydrous sandstone was proposed to assess the failure state of hydrous sandstone in real time. Consequently, real time and portability requirements in structural monitoring can be met. The visual warning color order was screened via an EEG experiment and was determined to be reasonable for warning geotechnical engineering staff.

Acknowledgements

The authors would like to thank the project supported by the National Natural Science Foundation of China (Grant No. 61573073) and the Chongqing City frontier general and applied basic research projects (Project No. cstc2015jcyjA40008).

References

1. Scruby CB. An introduction to acoustic emission. Journal of Physics E Scientific Instruments. 1987;20:946.
2. Sun Q. The influence of moisture content on the acoustic emission at threshold of rock destruction. Acta Geodynamica Et Geomaterialia. 2015:279-87.
3. L. Girard, S. Gruber, S. Weber, J. Beutel. Environmental controls of frost cracking revealed through in situ acoustic emission measurements in steep bedrock. Geophysical Research Letters. 40 (2013) 1748–53.
4. S. Chen, L. Liang, Y. Tian. The number of connected components in a graph associated with a rectangular (0,1)-matrix. Linear Algebra & Its Applications. 487 (2015) 74-85.
5. E.S.A.D. Silva, H. Pedrini. Connected-component labeling based on hypercubes for memory constrained scenarios. Expert Systems with Applications. 61 (2016) 272-81.
6. Suzuki T, Shiotani T, Ohtsu M. Evaluation of cracking damage in freeze-thawed concrete using acoustic emission and X-ray CT image. Construction & Building Materials. 2017;136:619-26.
7. Wan LH, Ping C, Huang YH, Wang YX. Study of subcritical crack growth of rocks and threshold values in different environments. Rock & Soil Mechanics. 2010;31:2737-42.
8. Costa ET, Costa EQ. Changes in EEG amplitude (Alpha and Beta waves) with Thermal environment. 2016;83:page. 87-93.
9. Münch M, Plomp G, Thunell E, Kawasaki A, Scartezzini JL, Herzog MH. Different colors of light lead to different adaptation and activation as determined by high-density EEG. Neuroimage. 2014;101:547.
10. Alharbi ET, Alharbi ET, Alharbi ET. SINGLE TRIAL CLASSIFICATION OF EVOKED EEG SIGNALS DUE TO RGB COLORS. Brain Broad Research in Artificial Intelligence & Neuroscience. 2017.